Microsc. Microanal. Microstruct. **1** (1990) 443–454 OCTOBER/DECEMBER **1990**, PAGE 443

Classification
Physics Abstracts
07.80 — 29.30 — 29.70 — 81.00

Analytical electron microscopy at the atomic level with parallel electron energy loss spectroscopy

Danièle Bouchet([1]), Christian Colliex([1]), Parmjit Flora([1]), Ondrej Krivanek([2]), Claudie Mory([1]) and Marcel Tencé([1])

([1]) Laboratoire de Physique des Solides, Université Paris-Sud, Bâtiment 510, 91405 Orsay Cedex, France
([2]) Gatan Research and Development, 6678 Owens Drive, Pleasanton, Ca 94588, U.S.A.

(Received October 01, 1990; accepted February 02, 1991)

Résumé. — La caractérisation d'échantillons solides à l'échelle atomique passe par l'implantation de diverses spectroscopies sur la colonne d'un microscope électronique. C'est possible en particulier en associant une sonde de petite taille et de grande brillance dans un STEM avec une détection parallèle du signal de perte d'énergie. Cet article décrit deux situations typiques en science des matériaux, où le signal analytique (présence d'un seuil, modification de structures fines) est utilisé à l'échelle du nanomètre. Le premier exemple concerne l'identification chimique par l'intermédiaire du seuil O_{45} de petits agrégats de thorium qui peuvent être réduits à des atomes isolés. Le second vise à détecter du soufre en ségrégation le long de coeurs de dislocations dans un joint de grains bien défini. Le soufre n'est pas trouvé, mais on enregistre des changements de structures étendues après le seuil, qui peuvent être reliés à des modifications de l'environnement cristallographique local.

Abstract. — For an improved exploration of the nanoworld at the atomic level, the implementation of various spectroscopies on an electron microscope column broadens the range of available information. Characterization at the atomic level is now made possible by an efficient combination of STEM probes of small size and high brightness with a parallel array of detectors for the EELS signal. The present paper describes two typical situations in materials science, where this analytical signal (presence of a given edge, change in the fine structures) is used at the nanometer (or subnanometer) scale. The first one is the chemical identification of small clusters of thorium (down to the single atom size) through the occurrence of the O_{45} edge. The second one is the search for sulphur along isolated dislocation cores within a well characterized grain boundary. Sulphur is not detected but changes in extended fine structures can be related to local variations of crystallographic environment.

1. Introduction.

When considering any type of specimen with inhomogeneities at the scale of a few interatomic distances, such as encountered in materials science, in chemical reactions, or in molecular biology, it is of prime importance to measure a wide range of local properties. Beyond visualizing the

external topography, and determining the local geometrical arrangement through high resolution images and nano-diffraction patterns, the addition of spatially resolved spectroscopies on electron microscope columns broadens the range of available information (chemical composition, electronic properties...). This improved exploration of the nanoworld at the atomic level is the fundamental goal for developing analytical electron microscopy tools at their limit. The present contribution illustrates, using practical examples, the field of experiments now accessible with the implementation of parallel electron energy loss spectroscopy (PEELS). This device is mounted on a dedicated scanning transmission electron microscope (STEM) equipped with a field emission gun. This paper can be considered as an updated version of two previous ones dealing with the same general topic: "*Frontiers of analytical electron microscopy in materials science*" [1,2].

The major signals of interest for the chemical characterization of thin foils are electron energy loss spectrum (EELS) and X-ray emission spectrum (EDX). In both cases, the presence of a given element is identified through the occurrence of a specific feature (line or edge), which is due to an excitation of a core level and which lies on top of a smoothly varying background. In the case of EELS spectra, which is the subject of this paper, the measurement of an integrated signal is required for quantitative local analysis. Furthermore, the detailed spectral distribution of an ionization edge as a function of energy loss with both near edge and extended structures conveys extra information about the local bonding and arrangement of the excited atom. The shape of the near edge structures (ELNES) over the first 10-20 eV above threshold can be used as a fingerprint of the first coordination shell, cluster symmetry and local charge transfer with the ligands. The long range oscillations over the next 100-300 eV (EXELF) can be analyzed in terms of a radial distribution function.

2. Instrumental considerations.

2.1 THE STEM DESIGN AND THE PROBE FUNCTION. — In order to investigate the spatial dependence of an inelastic event, the imaging lens of the electron microscope is an essential component. The STEM configuration is very well adapted. As shown in figure 1 the objective lens provides a sharply focused probe of high incident energy electrons ($\simeq$ 100 keV) on the entrance surface of the specimen.

With a field emission gun in the VG-HB 501, subnanometer incident probes are reproducibly obtained (Mory *et al.* [3]). Recent progress in lens design with lower C_s values have resulted in very small probes of $\simeq$ 0.2 nm in diameter [4]. The volume of signal generation is ultimately governed by the area covered by the incident beam and by the specimen thickness. The problem of beam spreading through thick foils has been extensively discussed in connection with the spatial resolution attainable in EDX measurements: it has been shown that a useful compromise in terms of signal to noise ratio is reached when the extent of beam broadening is equivalent to the size of the incident probe (see Garratt-Reed [5]). In the EELS case, the collimation effect set by the entrance aperture of the spectrometer on the transmitted beam reduces the importance of thickness effect. Besides plural scattering events in thick sections prevent from clear detection of the core-edge signals. Consequently, for high spatial resolution EELS measurements, thin sections are recommended, very similar to those used in high resolution microscopy (HREM). The analytical point spread function is then very close to the incident probe function, if we neglect a typical 0.2-0.3 nm delocalization contribution for typical 100 eV losses (Mory *et al.* [6]).

2.2 THE PARALLEL EELS COMPONENT. — Another major aspect of the STEM design lies in the highly efficient multidetector strategy. For each probe position on the specimen, various ring detectors can collect electrons scattered to large angles, mainly through elastic processes. These

signals are very useful to visualize the areas scanned by the primary electron beam. Simultaneously, the energy of the forward transmitted beam is analyzed by a magnetic spectrometer and the EELS spectrum recorded on an array of detectors. In such a parallel EELS mode, the whole spectrum is measured simultaneously and the intrinsic advantages of a parallel detection system as compared to serial collection can clearly be demonstrated [7]. In the present work, we use the Gatan system developed by Krivanek *et al.* [8]. Its basic components are the magnetic sector with the floating potential tube (for absolute calibration of energy losses), the post spectrometer lens assembly (made of three quadrupoles) and the photodiode detection system (consisting of a YAG screen, a fiber-optic window and a photodiode array). Finally a thermoelectric cooler is used to reduce detector noise. These are shown schematically on the upper part of figure 1.

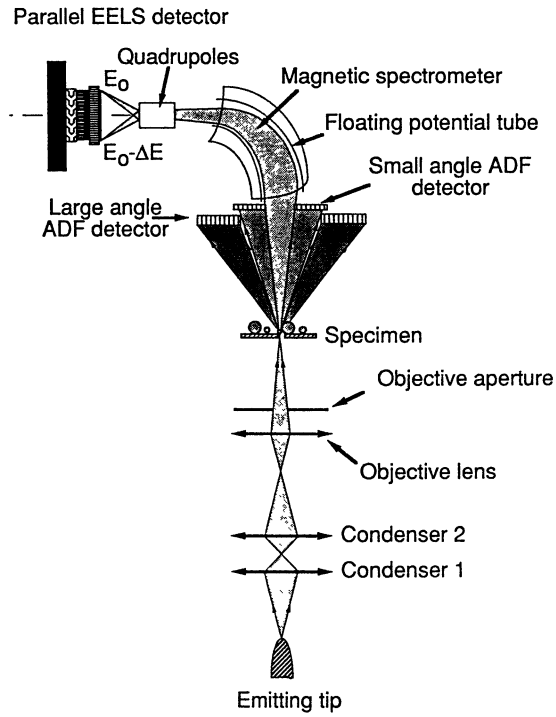

Fig. 1. — Schematic diagram of the VG-STEM column equipped with the Gatan PEELS device.

For quantitative use of EELS spectra, two steps are required: 1) edge identification and 2) edge measurement. When analysing small concentrations of a given element through edges of low intensity between $\simeq$ 100 and 500 eV loss, the recorded signal is very weak, superposed on an intense background and therefore exhibits a small jump ratio at threshold. Furthermore, the channel-to-channel gain variation of the detector (around 1% rms) contributes to the poor detectability of weak signals.

In order to improve on these limitations, several specific spectral processing techniques have been developed, the most elaborate one being the gain averaging method due to Shuman and Kruit [9]. A simpler way of stripping away the detector response is to record first-, second- and higher- order difference spectra. As explained in [8], it is done by acquiring, in rapid succession,

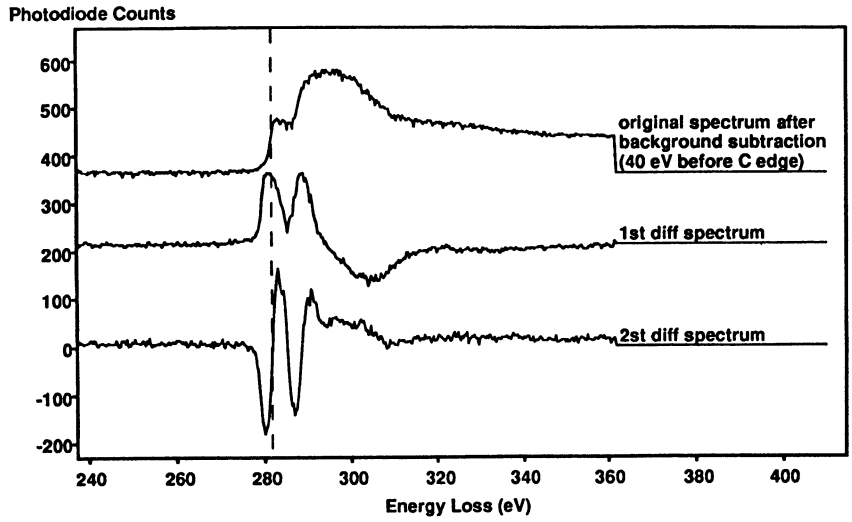

Fig. 2. — Reference carbon K-edges recorded from $a \simeq 3$ nm thin layer used for supporting small particles.

spectra which are shifted in energy by a small amount, and by calculating their differences. Figure 2 shows the well-known carbon K-edge for a thin foil of amorphous carbon (thickness $\simeq$ 3-5 nm) which is used as a supporting layer for many specimens made of small particles. It also contains the first and second difference spectra which clearly reveal changes in slopes and inflexion points.

Another important trend for EELS quantifications is to fit experimental spectra with model spectra built from linear combinations of reference edges due to test specimens or to *a priori* computations (Shuman and Somlyo [10], Leapman and Swyt [11], Manoubi *et al.* [12]). For very low concentrations, Shuman and Somlyo [10] have demonstrated the advantage of achieving this fitting technique on difference spectra. Consequently, it is of prime interest to store in the computer memory libraries of reference spectra, not only in the normal $N(\Delta E)$ mode such as already compiled in the EELS atlas [13], but also in the difference modes. Of course, difference spectra can always be numerically derived from normal spectra, but with higher systematic noise than spectra directly recorded in the difference mode. Figure 2 constitutes one step in this direction: the first difference spectra of the carbon K edge will be used, in the following section, to normalize and analyse spectra recorded on small metallic clusters deposited on these supporting layers.

3. PEELS spectroscopy on quasi-atomic clusters.

Small metallic clusters made of staining products generally used for visualizing biomolecules supported on thin amorphous films constitute a useful test specimen to evaluate the ultimate sensitivity of the PEELS technique in terms of minimum number of detectable atoms [14]. We report here some preliminary work on small clusters of thorium. An extended study on mixed specimens made of two components (uranium/ terbium or uranium/thorium) will be published in a forthcoming paper. The specimen topography is schematically shown in figure 3.

When they do not decorate the DNA filament, heavy metal atoms form clusters of size ranging from isolated single atom up to 2 or 3 nm (i.e. made of a few hundred atoms). They can be easily visualized as white dots in the ADF micrograph (see Fig. 4).

The probe is located on selected clusters or between them, and spectra are acquired in the

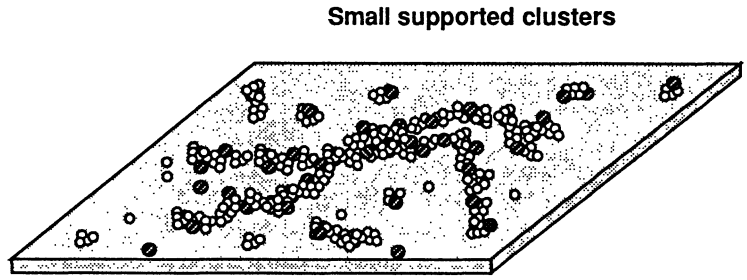

Fig. 3. — Schematic representation of small clusters of heavy metals used for staining supported biomolecules. Several types of atoms are shown, and one can find isolated atoms and clusters of different sizes.

Fig. 4. — ADF micrograph of small supported thorium atoms of different sizes selected for PEELS measurements.

PEELS mode. When fixed on top of a big cluster, the EELS spectrum clearly displays the two characteristic edges, for Th (O_{45} at 85 eV followed by a maximum at 95 eV) and for C (K-edge at 284 eV). See figure 5 where the signals after background subtraction are also shown. However for the smaller dots in the ADF image, the thorium edge is too faint for a correct background extrapolation following the conventional procedure.

Consequently, we have used the first difference mode as illustrated in figure 6 for the spectrum acquired on the big cluster and in figure 7 when positioning the probe on one of the smaller clusters in the ADF image. Note that the recorded small bump below $\simeq$ 100 eV disapears when moving the probe out of the cluster and reappears, of the same magnitude, when coming back on the cluster.

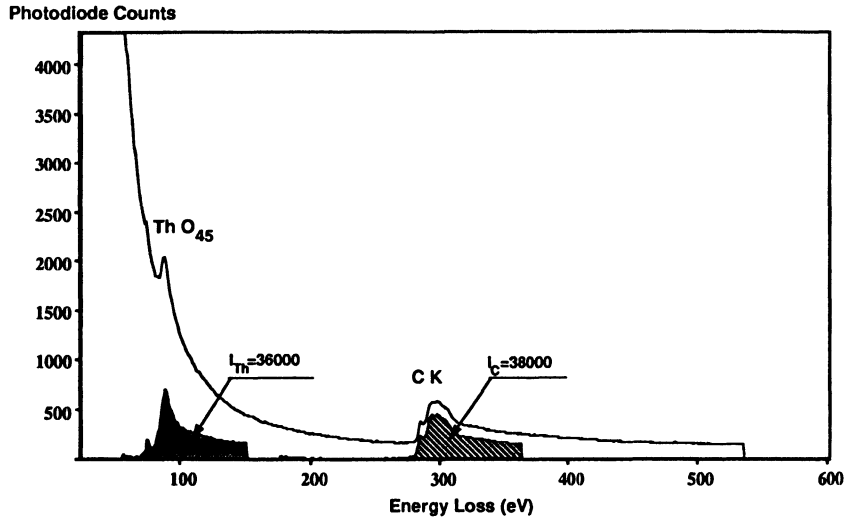

Fig. 5. — Spectrum $I(\Delta E)$ recorded from a large cluster: the analysed area contains $\simeq$10-50 atoms, as estimated from the conventional quantitative analysis method by comparison between the thorium O_{45} and the carbon K edges.

Furthermore, for different clusters producing ADF images of the order of the probe size ($\simeq$ 0.7–0.8 nm), the difference EELS signal on the thorium edge remains of the same order of magnitude. All spectra are scaled with the already mentioned signal for the carbon K-edge.

This behaviour suggest that the thorium signal is recorded from a few thorium atoms and in some cases could be from a single atom. In order to corroborate this interpretation, we have attempted to evaluate the number of thorium atoms responsible for this signal in several steps, using gross approximation, so that the final number is only estimated with a rather large error. The ratio between the number of thorium and carbon atoms in the spectrum of figure 5 is calculated with the simple formula:

$$\frac{N_{\mathrm{Th}}}{N_{\mathrm{C}}} = \frac{I_{\mathrm{Th}}}{I_{\mathrm{C}}} \times \frac{\sigma_{\mathrm{C}}}{\sigma_{\mathrm{Th}}}$$

The cross-section for carbon is well known, but that for the O_{45} edge of thorium is unknown. Extrapolating with simple arguments from compiled cross sections, we assume $\sigma_{\mathrm{C}}/\sigma_{\mathrm{Th}} \simeq 0.05$ in the experimental conditions, i.e. E_{o} =100 kV, α=25 mrad, Δ=70 eV. The second step is the

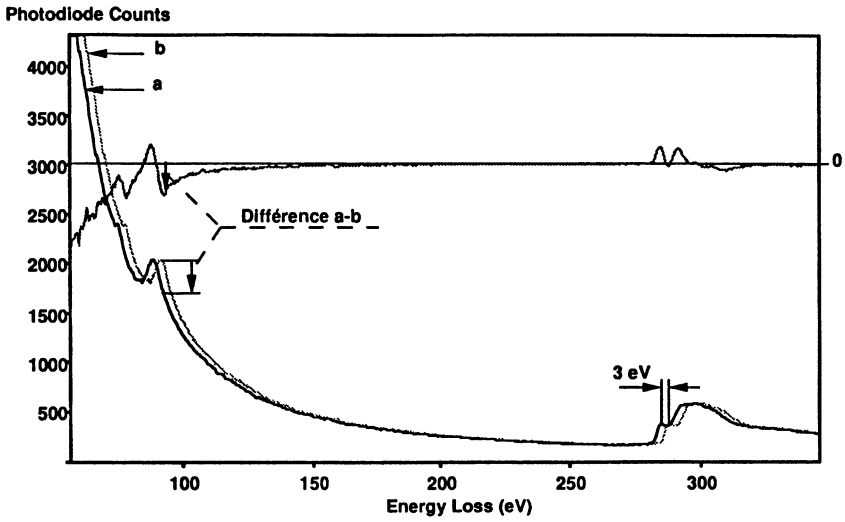

Fig. 6. — Numerical difference spectrum from figure 5 obtained by shifting the original spectrum by 3 eV.

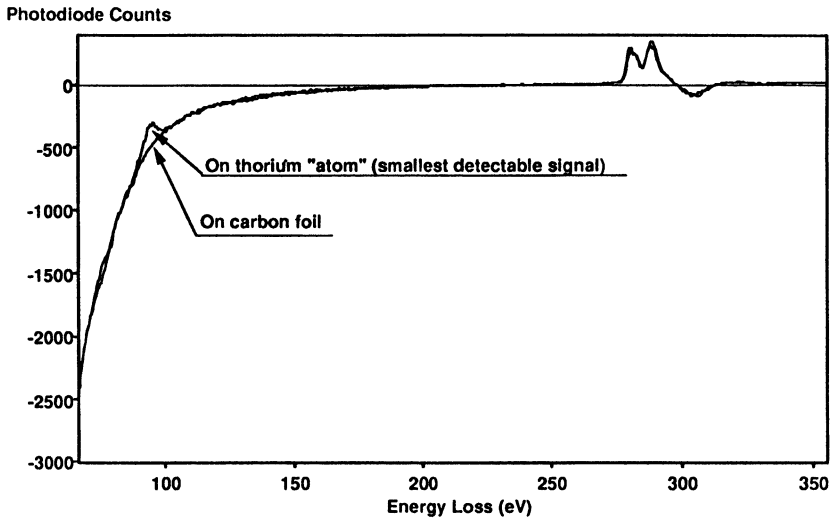

Fig. 7. — First difference spectra directly recorded from one of the smallest visible objects in the ADF image, and on the carbon layer nearby.

evaluation of the number of carbon atoms in the analysed area. The thickness is evaluated through the ratio of the zero-loss peak to the total intensity in the spectrum, and is of the order of 3 nm. Finally, the number of thorium atoms giving rise to the weak oscillation in figure 7 is deduced from the number of thorium atoms measured in figure 5. These show a clear oscillation in figure 6 after scaling the heights of the carbon peak in the difference spectra. Finally, combining all the uncertainties coming, we have estimated that the smallest recorded thorium O_{45} signal would correspond to a number of thorium atoms between 0.5 and 3. It is very difficult to be more accurate

at the present state of quantification but it is in reasonable agreement with the statement that EELS spectroscopy on a single atom is feasible.

4. Study of the equilibrium segregation of sulphur on grain boundaries in nickel.

4.1 STATEMENT OF THE PROBLEM. — The segregation of small amount of impurities to grain boundaries (GB) may significantly alter properties of the bulk materials, such as embrittlement and intergranular corrosion susceptibility. We have been working for a while on the segregation of sulphur at grain boundaries in high purity nickel with the aim of understanding the relation between the grain boundary structure and the presence and amount of segregation. Only the equilibrium segregation, which is schematically presented in figure 8, is considered here. In a simple model, the segregated impurities lie on 1 or 2 atomic planes, i.e. typically on a 0.5 nm layer at the interface. The identification and measurement of such submonolayer concentrations require a very high level of instrumental performance. In a first step the small number of atoms to be detected within the reduced analysed volume needs optimum working conditions, in terms of spatial resolution and beam specimen interaction conditions.

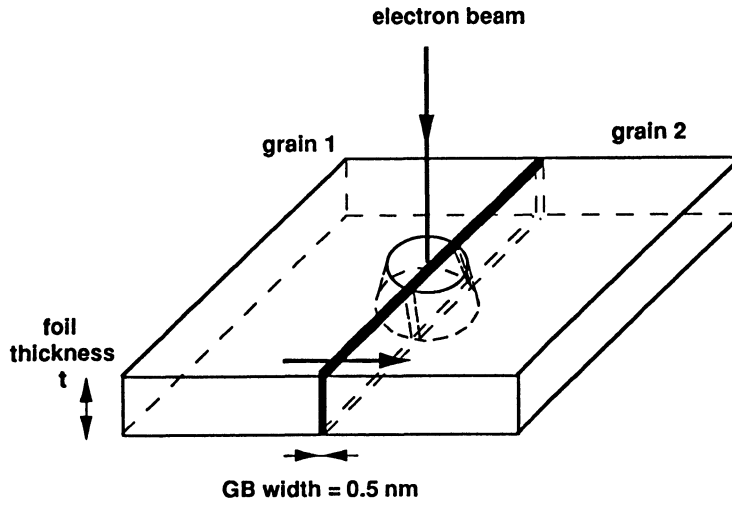

Fig. 8. — Simplified model of a planar interface between two crystrals. The analysis is performed for different positions of the incident probe across the GB as indicated by the arrow. An equilibrium segregation would be represented by a delta function of the grain boundary width.

In a polycrystalline specimen, the probability of finding the right GB in a thin area with the correct inclination is very poor. Only very few data have been obtained, and generally on rather thick sections ($t \simeq 100$ nm). For instance, a weak EDX line of sulphur corresponding to an atomic concentration of 0.5-0.6% of sulphur within a cylindrical analysed volume of about 10-15 nm in diameter has been measured on several general grain boundaries [15]. To further interpret this type of result, we have to consider the fact that the typical dimension over which equilibrium segregation occurs, is generally smaller than the probe function. Consequently, the concentration of impurities at the grain boundary itself can only be deduced from the measured signal through an extra step of data processing. It may involve either a deconvolution of the analytical point

spread function, or modeling the distribution of segregated atoms, generally an homogeneous planar layer, and comparing simulated spectra with experimental ones.

With this assumption, the EDX data would correspond to a typical segregation of S along the general GB, equivalent to a fraction of a monolayer, typically between 10 and 40% [16]. However, the experimental situation was not sufficiently clear to understand the fundamental relation between GB microstructure (with its long range parameters: misorientation, GB plane, rigid body translation, and local defect content) and the importance of segregation.

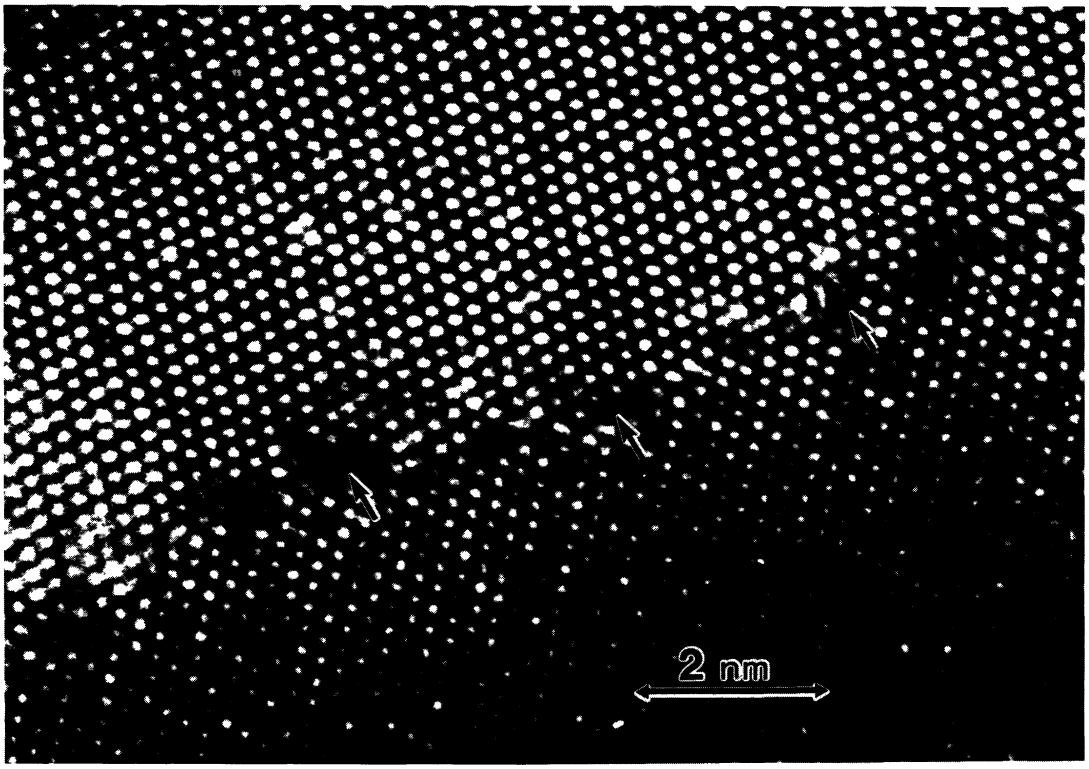

Fig. 9. — HREM micrograph of the grain boundary at the end of the bicrystal, supposed containing segregations of sulphur. At this scale it is not a straight interface but a succession of dislocation cores about 1-2 nm apart (micrograph courtesy of J. Thibault, CENG Grenoble). Analysis in the STEM is performed by positioning the primary probe on such individual dislocation cores visible as white contrast zones in the ADF image.

4.2 AN IMPROVED SPECIMEN CONFIGURATION. — A nickel bicrystal has been grown with a tilt $\Sigma 11$ GB corresponding to a 50°48 angular deviation around the <110> common rotation axis. The nominal concentration in sulphur is <10 ppm. During the solidification process sulphur segregation occurs at the end of the bicrystal as evidenced by Auger analysis on a fracture surface [17]. TEM thin specimens have been prepared across the grain boundary near the end of the bicrystal where segregation of S is expected from Auger measurements.

HREM observations realized on the 400 kV Jeol microscope in CENG-Grenoble clearly de-

monstrate that the model of planar interface and homogeneous segregated layer along the grain boundary is questionable. As shown in figure 9, the GB is actually constituted of a sequence of defects (dislocations) with an average distance of 1-2 nm apart, connected with stretches of perfect planar interface.

The same specimen has been observed with the VG-STEM in Orsay and PEELS spectra have been acquired while focusing a typical 1 nm probe (with 1 nA current) both on the matrix and on selected intergranular dislocations. Through they are not of high quality, the ADF images continuously visualized during spectrum recording constitute a useful way for checking the stability of the beam position over the isolated defect.

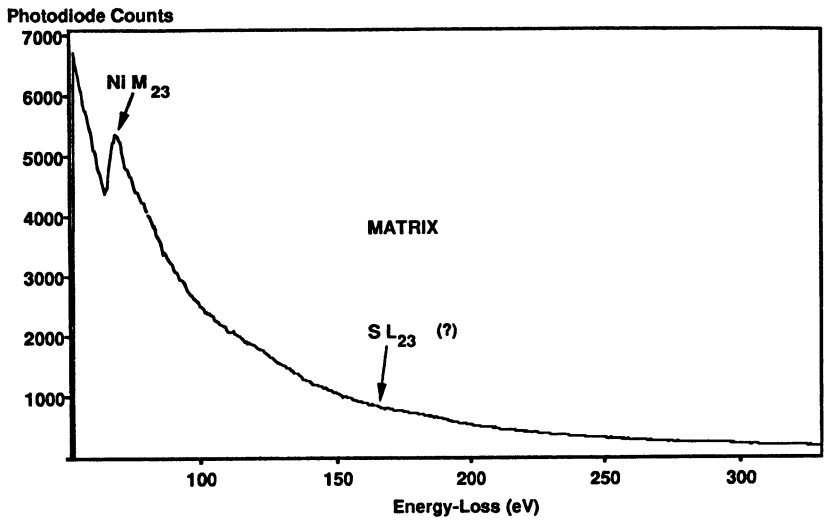

Fig. 10. — M_{23}-edge of nickel in the normal $I(\Delta E)$ PEELS mode. The fine oscillating structures (EXELFS) prevent simple modeling of the background in the energy loss range supposed to contain the sulphur L_{23} signal.

4.3 RESULTS OF PEELS ANALYSIS AND DISCUSSION. — For a pure nickel foil, the M_{23} edge appears with a sharp threshold at $\simeq$68 eV and its contribution extends with weak EXELFS oscillations over a few hundred eV (see Fig. 10). In particular, the energy loss background due to the nickel matrix cannot be fitted with a simple model over the 100-200 eV, where the characteristic sulphur L_{23} signal has to be searched. From the EELS atlas, this edge in pure sulphur is a delayed one with an onset at $\simeq$165 eV and a maximum around 200 eV. The results are gathered in the four spectra of figure 11: there is a reference spectrum from nickel-oxide standard; a reference spectrum from the nickel matrix and two spectra recorded when focussing the incident probe on two distinct dislocation cores along the grain boundary.

There is no clearly identifiable sulphur edge on the intergranular dislocations, but one detects obvious differences in EXELFS fine structures when compared to the matrix. Below $\simeq$110 eV, the matrix and GB spectra exhibit rather similar oscillations, of weaker amplitude however on the dislocation cores. The differences are more noticeable in the energy loss range 110-150 eV where the clear bumps for the matrix are not detectable on the GB defect. We are presently trying to analyse these oscillations in terms of radial density distribution, but quantitative reliable

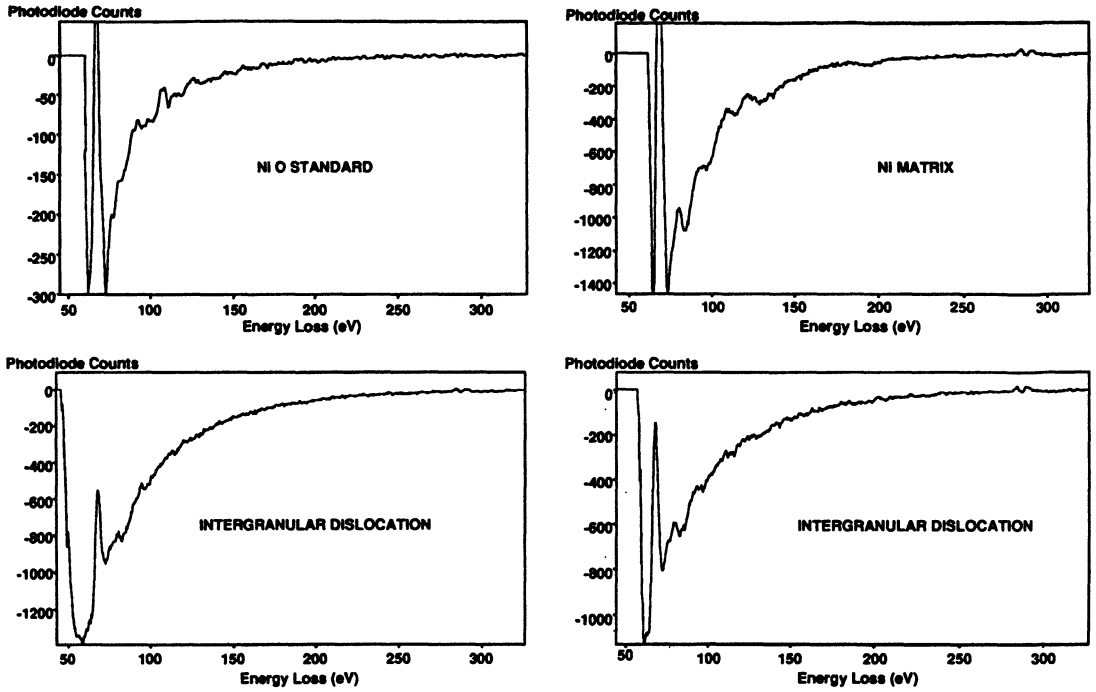

Fig. 11. — A selection of first difference edges either used for reference (Ni matrix and NiO) or recorded on two distinct intergranular dislocations. In each case, the analysed area is of the order of 1 nm^2.

data are not yet available. We can only suggest that the decrease of the EXELFS oscillations amplitude (which is more intense at higher energy losses) reflects disorder and broadened range of interatomic distances within the analysed volume, that is typically a cylinder of 1 nm in diameter along the dislocation core.

These results can then be interpreted either with:
• "the sulphur is not detected because its local concentration remains below the detection limit which is estimated to be of the order of 0.5 % atomic concentration in volume for the experimental condition used";
or with
• "the sulphur atoms are removed by radiation damage during the analysis. The dose for recording the spectra is actually $\simeq$1-2$\times$ $10^{10}e^{-}/nm^2$. The disorder observed by changes in EXELFS structures could then be regarded as a "print" of the presence of sulphur atoms which have been sputtered under the beam".

More generally, this study demonstrates the intrinsic possibility of performing edge fine structure analysis on single defects.

5. Conclusion.

The examples described in this paper show that the instrumentation nowadays available offers the possibility of analytical investigations concerning the atomic-level microstructure of inorganic solids: clusters of a few atoms, isolated defects in solids... The quantitative analysis of the data however requires further work, in order to evaluate more accurately the number of atoms of a given type within a selected cluster, or the extent of structural disorder within the selected defect.

Acknowledgements.

The authors thank E. Delain (Inst. G. Roussy, Villejuif, France) for preparing the specimens of small metallic clusters, M. Biscondi (Ecole Nat. Sup. Mines de St Etienne, France) et W. Swiatnicki (Polytechnic School, Warsaw, Poland), respectively for the elaboration of the Ni bicrystal and for the preparation of EM thin foils, J. Thibault (CENG, Grenoble, France) for her assistance in the HREM observations of the nickel bicrystal.

References

[1] COLLIEX C., *Ultramicroscopy* **18** (1985) 131.
[2] COLLIEX C., MAURICE J.L., UGARTE D., *Ultramicroscopy* **29** (1989) 31.
[3] MORY C., TENCÉ M., COLLIEX C., *J. Microsc. Spectrosc. Electron* **10** (1985) 381.
[4] PENNYCOOK S.J., *Ultramicroscopy* **30** (1989) 58.
[5] GARRATT-REED A.J., Scanning Electron Microscopy, SEM Inc., AMF O'Hare, II. 60666, USA, I (1985) 21.
[6] MORY C., KOHL H., TENCÉ M., COLLIEX C., to be published in *Ultramicroscopy* (1991).
[7] EGERTON R.F., *J. Electron. Microsc. Techn.* **1** (1984) 37.
[8] KRIVANEK O.L., AHN C.C., KEENEY R.B., *Ultramicroscopy* **22** (1987) 103.
[9] SHUMAN H., KRUIT P., *Rev. Sci. Instrum.* **56** (1985) 231.
[10] SHUMAN H., SOMLYO A.P., *Ultramicroscopy* **21** (1987) 23.
[11] LEAPMAN R.D., SWYT C.R., *Ultramicroscopy* **26** (1988) 393.
[12] MANOUBI T., TENCÉ M., WALLS M.G., COLLIEX C., *Microsc. Microanal. Microstruct.* **1** (1990) 23.
[13] AHN C.C., KRIVANEK O.L., An Atlas of Electron Energy Loss Spectra, available from the secretary. Center for Solid State Science, ASU, Tempe, Az.85287 (1982).
[14] MORY C., COLLIEX C., *Ultramicroscopy* **28** (1989) 339.
[15] BEAUNIER L., BOUCHET D., COLLIEX C., TREBBIA P., VIGNAUD C., *J. Microsc. Spectrosc. Electron.* **10** (1985) 453.
[16] BEAUNIER L., VIGNAUD C., BOUCHET D., COLLIEX C., TREBBIA P., *J. Phys.Colloq. France* **46** (1985) C4-405.
[17] SWIATNICKI W., LARTIGUE S., BISCONDI M., BOUCHET D., *J. Phys. Colloq. France* **51** (1990) C1-341.